Tribology and Materials
Vol. 3, No. 3, 2024, pp. 141-149
ISSN 2812-9717
https://doi.org/10.46793/tribomat.2024.011

Investigations on dry sliding wear and friction behaviour of alloy steel obtained by powder metallurgy

Kathhi Palaksha REDDY, Thanjavur Krishnamoorthi KANDAVEL, Balaraman PANNEERSELVAM, Sreehari V. MADHAVAN*

School of Mechanical Engineering, SASTRA Deemed University, Thanjavur, India
*Corresponding author: sreehari_vm@mech.sastra.edu

Keywords

powder metallurgy
prealloyed powder
sliding wear
Atomet 4601

History

Received: 14-06-2024
Revised: 21-07-2024
Accepted: 26-07-2024

Abstract

The present work investigates the dry sliding wear and friction behaviour of an alloy steel developed through powder metallurgy. Prealloyed Atomet 4601 powder was thoroughly mixed with elemental powders of 0.35 C, 0.25 Mn, 0.1 Si and 0.9 Cr (in wt. %) to create this alloy steel, whose composition closely matches EN24 (AISI 4340) wrought steel. The dry sliding friction and wear test experiments were performed in a pin-on-disc tribometer. For the various cases considered in friction and wear tests, the wear rate is lowest (0.32×10^{-3} mm^3/m) at 15 N and 1.77 m/s and highest (1.02×10^{-3} mm^3/m) under severe conditions of 32.5 N and 2.83 m/s. The coefficient of friction is highest (0.673) at 15 N and 0.71 m/s and lowest (0.1311) at 32.5 N and 2.83 m/s. Subsequently, regression models are developed based on experimental results and the interaction effect of load and speed on the response parameters are plotted using MATLAB. An R^2 value of 0.98 indicates a strong correlation between the response and the input variables. X-ray diffraction (XRD) and optical and scanning electron microscope (SEM) analyses of the most worn specimens revealed carbides and oxides in the ferrite grain matrix, with adhesive, abrasive and oxidative wear being the primary mechanisms observed.

1. Introduction

Powder metallurgy (PM) is a technique in which powders can be processed to produce near-net-shape, high-quality complex parts at a low cost of manufacture. PM allows the creation of unique alloy combinations that are difficult to produce through traditional melting and casting techniques due to the segregation of particles, difficulty in uniform distribution of particles, precise control over gradient, etc. Sintered alloy steels can have a variety of material compositions including iron, nickel and other elements, which can be tailored to specific applications. Sintered alloy steels are widely used to make parts such as self-lubricating bearings, tungsten carbide cutting tools, grinding wheels, welding rods, gears, etc. PM steels are widely used in automobile and aerospace industries [1]. New PM alloys are being developed using powder forging to meet high-performance engineering requirements such as higher mechanical strength and wear resistance, better workability and corrosion resistance, etc [2].

Powders are mainly produced through solid-state reduction, atomisation, electrolysis and chemical methods. Alternative methods to develop new alloys through the PM route include employing admixed powders, diffusion-alloyed powders, prealloyed powders and hybrid alloy powders. In prealloyed powders, two or more distinct metal powders are prealloyed in advance, prepared by melt atomisation, with lesser segregation due to high cooling speeds. During sintering, all elements are homogenised. Each particle maintains a unique composition after heat treatment. Prealloyed powders can be used to make low-alloy steel powders for developing various near-net-shaped parts, such as HSS, heterogeneous alloys of Cu and Ni, with greater strength, hardness, etc. Atomet 4601 is a water-atomised prealloyed powder which is designed for high-strength and powder forging applications.

The wear and friction in sliding conditions depend on contact pressure, temperature, lubrication, alloying elements, density, hardness, tribochemical reactions, physical adsorption of active molecules on surfaces, roughness, material type, microstructure, etc. There is a greater need to understand the tribological performance of PM alloy steels in dry sliding operating conditions. Compared to wrought materials, PM parts experience higher wear over extended periods of relative motion. This leads to failure, dimensional changes and deterioration in the normal functioning of the parts. The wear and friction behaviour of sintered parts are extremely intricate and different from those of conventional solid parts due to built-in porosity [3].

Several researchers investigated wear in unlubricated sliding conditions of the sintered low-alloy steels. The addition of molybdenum enhances wear resistance in Fe-0.5C PM alloys more than the addition of copper [4]. The mass loss of Fe-0.5C sinter-forged PM materials of two density levels increased with operating parameters irrespective of densities. Soft ferritic-pearlitic microstructure causes uniform wear [5]. Li and Olofsson [6] studied the wear characteristics of wrought steel sliding on PM materials and PM sliding on PM parts. They observed the influence of the porosity of PM materials on the wear characteristics. Li et al. [7] investigated the mechanical, wear and corrosion performance of wrought and sintered cast iron. Increasing the Mn content in PM cast iron enhances its wear resistance due to increased hardness. Both alloys' corrosion behaviour remains the same, mainly due to austenite matrix formation. Singh and Grewal [8] observed that increasing load influences the wear performance more than the increased sliding speed of the AHC 100.29 iron powder-based ferrous PM preforms. The dominant wear mechanisms observed in the test samples were ploughing, micro-cutting and delamination. Several researchers have designed, analysed and optimised the sliding wear behaviour using response surface methodology [9-15].

Very few experimental investigations are reported on the development and performance of Atomet 4601 prealloyed powder-based low-alloy steels. The formation of carbides in Atomet 4601 + TiC alloy steel improved the hardness and significantly reduced the plastic flow [16]. Adding 2 wt. % titanium carbide elemental powder to Atomet 4601 enhanced the welding strength of the alloy steel under TIG welding [17]. Atomet 4601 + 0.35 C + 0.25 Mn + 0.1 Si + 0.9 Cr alloy has exhibited lesser densification owing to the work hardening and better aqueous and electrochemical corrosion behaviour compared to Atomet 4601 + 0.35 C [18].

The increase in tempering temperature led to the coarsening of martensite, which was responsible for the reduction in abrasive wear volume loss in EN24 steel. During the abrasive wear process, material removal occurred primarily through micro-ploughing and cutting mechanisms [19]. The wear volume loss of EN24 steel against aluminium alloy 6061 under lubrication conditions decreased with higher tempering temperatures due to martensite coarsening.

Microploughing and cutting were the main mechanisms of material removal [20]. Dhanvij et al. [21] performed wear tests on EN24 materials against an EN31 disc with varying loads (60 – 110 N) for 5 minutes at 1250 rpm, finding that the coefficient of friction initially increased with rubbing time before stabilising and both coefficient of friction and wear increased with higher loads. They also noted that carbon content fluctuations impacted the wear rate. The microhardness increased by over 4, 3.4 and 2.7 times, while wear resistance improved by approximately 1.8, 2 and 3 times from the base material for active screen plasma nitride-treated EN41B, EN8 and EN24 steels, respectively [22]. Dumne et al. [23] reported that load and speed have a significant influence on the wear rate of EN24 steel against oil-hardened non-shrinking steel under wet sliding conditions. As discussed in the author's previous research [18], the hardness of EN24 equivalent PM alloy was obtained as 16.7 HRC and while deformed (leading to less porosity) the hardness was measured to be 23.8 HRC. It is important to note that the EN24T wrought steel has a hardness of 24 HRC.

The literature survey reveals that researchers are yet to explore the effect of reinforcing elemental powders and wear test variables, such as normal load and sliding speed, on the tribological behaviour of Atomet 4601-based alloy in detail. So, the present research aims to study the influence of normal load and sliding speed on the dry sliding friction and wear response of Atomet 4601 + 0.35 C + 0.25 Mn + 0.1 Si + 0.9 Cr (EN24 equivalent PM alloy) and perform microstructure evaluation of maximum worn-out sample surfaces using X-ray diffraction (XRD), optical and scanning electron microscope (SEM) analysis. The study also extends performing regression analysis of friction and wear characteristics of this alloy steel.

2. Experimental methodology

Atomet 4601 prealloyed powder is procured by Rio Tinto Metal Powders, Canada. In Atomet 4601, the elemental powders like manganese, molybdenum, nickel, iron, carbon and sulphur are already in an alloyed form, meaning the composition is homogeneously mixed at the atomic level. The prealloyed powder has a negligible amount of carbon. Based on the data sheet supplied by the producer, the chemical composition and sieve analysis are given in Tables 1 and 2, respectively. It is noted from Table 2 that most of the powder particles are larger than 45 µm in size.

EN24 (AISI 4340) is a wrought alloy steel with high tensile strength, wear resistance and toughness. It is used for crankshafts, propeller shafts, axles, gears, engine gearboxes, punches and dies. The chemical analysis of this alloy steel is given in Table 3.

In the present work, carbon and other elemental powders are added to the Atomet 4601 prealloyed powder to convert it into a PM alloy steel whose chemical composition (Atomet 4601 + 0.35 C + 0.25 Mn + 0.1 Si + 0.9 Cr wt. %) is close to EN24 alloy steel. The addition of alloying elements will imbibe further strength. The employment of the PM process instead of using the EN24 wrought steel is due to the fact that PM is a technique in which powders can be processed to produce complex parts closer to the final dimensions, reducing the need for secondary operations such as machining. Consequently, the waste of material can be reduced resulting in low cost of manufacture.

Atomet 4601 prealloyed powder was thoroughly mixed with other elemental powders (C, Mn, Si and Cr) using a ball mill to produce the alloy steel. The powder mixing process parameters are: rotation speed of 80 rpm, steel balls diameter of 10 mm, ball-to-powder mass ratio of 1:10, mixing time of 8 hours and volume of grinding media to the volume of the mill drum of 1:3. The physical properties of the alloy steel powder are: apparent density of 3.156 g/cm^3, tap density of 3.511 g/cm^3, flowability of 22.254 s/50g and theoretical density of 7.764 g/ cm^3 [18].

Table 1. Chemical analysis of Atomet 4601 powder

Element	C	Mn	Mo	Ni	Fe	O	S
wt. %	0.003	0.216	0.542	1.771	97.38	0.08	0.0076

Table 2. Sieve analysis of Atomet 4601 powder

Sieve size, µm	250	150	45	Pan
Retained amount, wt. %	traces	9.8	65.5	24.7

Cylindrical compacts of Ø 25 × 32 mm in size were obtained with an axial compaction pressure of 585 MPa using a hydraulic press. A thin layer of aluminium coating (Fig. 1a) was applied to the outer surface of green compacts. This coating offers surface protection from oxidation and other atmospheric reactions that can occur at high temperatures during sintering [4]. The coated and dried preforms were sintered (Fig. 1b) in batches with a soaking time of 120 minutes at 1100 ± 10 °C in a 2 kW programmable muffle furnace and air-cooled within the furnace.

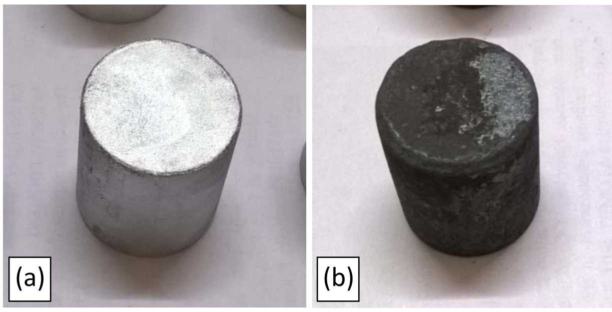

Figure 1. Cylindrical specimens: (a) aluminium-coated and (b) sintered

The as-sintered billet size was reduced to Ø 6 × 30 mm for use as test specimens through the wire EDM process. The pin's bottom surface was finished to a surface roughness of about *Ra* = 0.65 µm. They are paired with an EN31 steel counter-body disc of 55 HRC hardness, finished to a surface roughness of *Ra* = 0.8 µm. The friction and wear performance was studied according to ASTM G99 standard with a computer-based data acquisition system of a pin-on-disc test rig at a room temperature of about 30 – 32 °C and humidity of 75 – 80 %.

The test with 13 experimental trials was designed based on the central composite design technique of response surface methodology. Normal loads of 15, 23.75 and 32.5 N (i.e. applied pressure of 0.53, 0.84 and 1.15 MPa) and sliding speeds of 0.71, 1.77 and 2.83 m/s (i.e. 300, 750 and 1200 rpm) are the control factors used to study their influence on friction and wear behaviour.

Table 3. Chemical analysis of EN24 wrought alloy steel

Element	C	Mn	Si	Cr	Mo	Ni	S	P	Fe
wt. %	0.38 – 0.43	0.60 – 0.80	0.15 – 0.30	0.70 – 0.90	0.20 – 0.30	1.65 – 2.00	≤ 0.040	≤ 0.035	balance

Wear track diameter of 45 mm and test duration of 20 minutes were kept constant. The mass loss was estimated with a digital analytical balance with 0.0001 g accuracy by checking the mass of the pin at the beginning and end of the trial run. The coefficient of friction was recorded from the tribometer. Based on the experimental test results, regression models are developed and the interaction plots are generated.

The experimental trial, which gave the highest wear rate, was selected in each composition to characterise the worn-out surface morphology of the specimen. Kyowa ME-LUX-2 metallurgical microscope with a built-in CCD camera was used to obtain optical images. A Rigaku diffractometer with high intensity and nearly monochromatic CuKα rays was used to analyse the phase compositions. The microstructure of the highest wear test specimen was studied using SEM (JEOL JSM-6701F).

3. Results and discussion

3.1 Dry sliding friction and wear testing

Table 4 shows the experimental test results for wear rate and coefficient of friction (CoF) values for different input combinations of load and sliding speed. The obtained values of Table 4 are further used for developing a regression model for friction and wear characteristics.

Higher loads typically increase the wear rate due to elevated contact pressures, which can also impact the CoF. A smoother surface can reduce the CoF but might also affect the wear rate. Likewise, harder materials generally exhibit lower wear rates but can influence the CoF differently depending on the specific circumstances. The inclusion of various alloying elements and phases, such as carbide-forming elements, can increase hardness and reduce wear rates while influencing friction properties.

3.2 Regression modelling

Mathematical regression equations are developed to study the influence of input variables such as normal load and sliding speed and their interaction effect on the response parameters based on the experimental outputs of present alloy steel (EN24 equivalent PM alloy). The regression models, as given in Equations (1) and (2), can be employed to predict the friction and wear characteristics numerically for diverse inputs of sliding speed in m/s (*X*) and normal load in N (*Y*) using the limited experimental results.

Table 4. Dry sliding friction and wear test results

Test no.	Sliding speed, m/s	Normal load, N	Wear rate, mm^3/m	CoF
1	0.71	15	0.00049	0.67302
2	1.77	15	0.00032	0.55093
3	2.83	15	0.00040	0.47163
4	0.71	23.75	0.00064	0.54349
5	1.77	23.75	0.00041	0.48881
6	1.77	23.75	0.00042	0.49114
7	1.77	23.75	0.00043	0.49727
8	1.77	23.75	0.00043	0.48123
9	1.77	23.75	0.00045	0.50013
10	2.83	23.75	0.00048	0.17794
11	0.71	32.5	0.00092	0.57872
12	1.77	32.5	0.00062	0.47536
13	2.83	32.5	0.00102	0.13110

$$\begin{aligned}\text{Wear rate} &= -3.16447\cdot10^{-4} + 7.62014\cdot10^{-4}X + \\ &+ 7.17393\cdot10^{-5}Y - 8.36727\cdot10^{-5}XY - \\ &- 1.08959\cdot10^{-4}X^2 - 5.85514\cdot10^{-7}Y^2 + \\ &+ 1.14428\cdot10^{-5}X^2Y + 1.01656\cdot10^{-6}XY^2, \end{aligned} \tag{1}$$

$$\begin{aligned}\text{CoF} &= 1.31519 - 0.31958X - 0.052868Y + \\ &+ 0.0189XY + 0.089743X^2 + \\ &+ 7.93614\cdot10^{-4}Y^2 - 7.2138\cdot10^{-3}X^2Y. \end{aligned} \tag{2}$$

The ANOVA outcome for the wear rate of the alloy steel is listed in Table 5 at a 95 % confidence level. The sum of squares (SS), degree of freedom (DF) and mean square (MS) are presented. The model is significant, as the p-value for wear rate was obtained as 0.0004. The ANOVA outcome for CoF of the alloy steel is listed in Table 6 at a 95 % confidence level. The model is significant, as the p-value for CoF was obtained as < 0.0001. The obtained R^2 value is 0.98 for both wear rate and CoF, which reveals the strong correlation between the response and the independent parameters.

Table 5. ANOVA for wear rate (R^2 = 0.9838)

Source	SS	DF	MS	F-value	p-value	Contribution, %
Sliding speed	1.28×10^{-8}	1	1.28×10^{-8}	7.48	0.0410	5.88
Normal load	4.50×10^{-8}	1	4.50×10^{-8}	26.30	0.0037	20.68
Sliding speed × normal load	9.02×10^{-9}	1	9.02×10^{-9}	5.27	0.0701	4.15
Sliding speed^2	9.24×10^{-8}	1	9.24×10^{-8}	54.01	0.0007	42.47
Normal load^2	2.38×10^{-8}	1	2.38×10^{-8}	13.94	0.0135	10.96
Sliding speed^2 × normal load	1.68×10^{-8}	1	1.68×10^{-8}	9.86	0.0257	7.76
Sliding speed × normal load^2	9.07×10^{-9}	1	9.07×10^{-9}	5.30	0.0695	4.17
Residual	8.55×10^{-9}	5	1.71×10^{-9}			3.93
Total	2.18×10^{-7}	12				100

Table 6. ANOVA for CoF (R^2 = 0.98)

Source	SS	DF	MS	F-value	p-value	Contribution, %
Sliding speed	0.17	1	0.17	192	0.0001	73
Normal load	0.003	1	0.003	3.2	0.124	1.23
Sliding speed × normal load	0.015	1	0.015	16.9	0.006	6.44
Sliding speed^2	0.023	1	0.023	25.9	0.002	9.87
Normal load^2	0.010	1	0.010	11.4	0.014	4.29
Sliding speed^2 × normal load	0.007	1	0.007	7.51	0.033	2.87
Residual	0.005	6	0.0008			2.3
Total	0.233	12				100

3.3 Interaction plots for wear rate

The interaction plots obtained for the analysis of the wear rate are shown in Figure 2. The figure shows the effect of independent variables such as sliding speed and normal load on wear rate. Both the sliding speed and normal load have a significant effect on wear rate. An increase in speed initially reduces mass loss. However, as speed continues to increase, thermal softening dominates and enhances metallic contact, causing large-scale plastic deformation and severe wear. For a normal load increase from 15 to 32.5 N, the wear rate rose from 0.32×10^{-3} to 1.02×10^{-3} mm^3/m. The figure also indicates optimal input parameter values for wear rate. The wear rate is the lowest (0.32×10^{-3} mm^3/m) at 15 N and 1.77 m/s. The alloy steel could withstand the wear rate of 1.02×10^{-3} mm^3/m at severe operating conditions of 32.5 N and 2.83 m/s due to the presence of carbides, as observed in the XRD study results. Also, this better wear resistance is supported by the better workability and corrosion behaviour of this alloy steel as shown by Reddy et al. [18].

The inherent porosity in PM materials leads to complex wear patterns at the contact surfaces. The wear debris, once removed from the parent surface, accumulates in the pores on the worn surface of the compacts. With increased load, contact area increases and mild oxidative to severe metallic wear occurs at a given speed, aligning with the wear principle. Wear debris changes its size from fine to large. This phenomenon occurs on the contacting surface due to the delamination of the oxide layer, which accelerates the wear rate during testing [24]. Hence the interaction plots of wear rate are significant.

It is important to understand that adhesive wear is regulated by the adhesive strength of the interfaces and the plastic shearing of subsequent layers. As the softer pin slides on the counter-body disc, it may fuse and stick to the disc due to opposing forces. When sliding continues, these fused joints break off into unevenly shaped debris, resulting in adhesive wear [25]. Wear also occurs when the surfaces of the pin and counter-body disc experience dislocation, fracture and deformation. This leads to subsurface crack growth, the formation of craters and shear forces, resulting in the creation of long, thin flakes or laminates [26].

3.4 Interaction plots for CoF

The friction increases heat generation for any component that is in relative motion. So, the study of this phenomenon through interaction plots of CoF is very important. The interaction plots for the analysis of the friction behaviour are shown in Figure 3. The figure shows the influence of independent variables such as sliding speed and normal load on CoF. CoF is the highest (0.673) at 15 N and 0.71 m/s. Contact surfaces experience higher friction at the beginning since the disc is polished. Then, the coefficient of friction starts decreasing with increased sliding speed and normal load. At the highest normal load (32.5 N) and sliding speed (2.83 m/s), CoF is the lowest (0.1311) as thin oxide layer worn particles are continuously removed due to more oxidation of the interface material layers at high interface temperature [13,27]. Compared to load, sliding speed has more influence on CoF.

3.5 X-ray diffraction study

The Rigaku diffractometer was used to determine the different phases of materials by analysing the diffraction patterns produced when nearly monochromatic and high-intensity CuKα rays are scattered by the sample for different 2θ angles. The prealloyed powder Atomet 4601 contains 0.216 wt. % Mn, 0.542 wt. % Mo and 1.771 wt. % Ni. Figure 4 shows the Bragg peaks in the XRD pattern of alloy steel specimen with the highest wear.

In the XRD pattern, prominent peaks were found at around the diffraction angle 2θ = 30, 43, 62 and 74°, which demonstrate the presence of hematite (Fe_2O_3), the common form of iron oxide. The peak around 2θ = 20° indicates the presence of some magnetite (Fe_3O_4). The sharpness of XRD peaks suggests that the iron oxide particles present in the powder are crystallites. The broadening of the peaks seen in the XRD pattern is due to the presence of multiple phases having smaller crystallite sizes. Other prominent peaks of iron carbide (Fe_3C), manganese oxide (MnO_2), silicon dioxide (SiO_2) substrate iron (Fe) and traces of C and Si also could be observed.

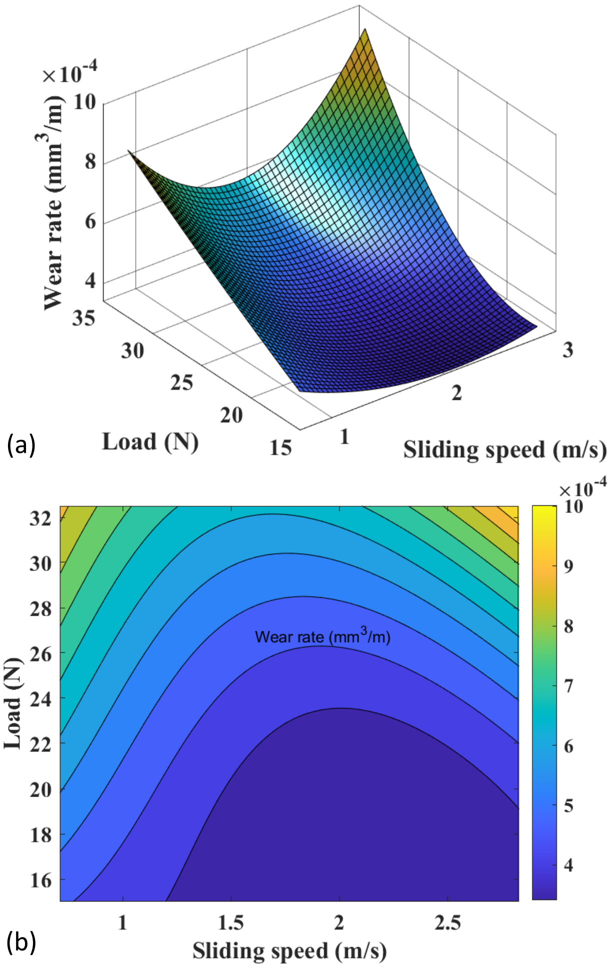

Figure 2. Interaction plots for wear rate: (a) 3D surface plot and (b) 2D contour plot

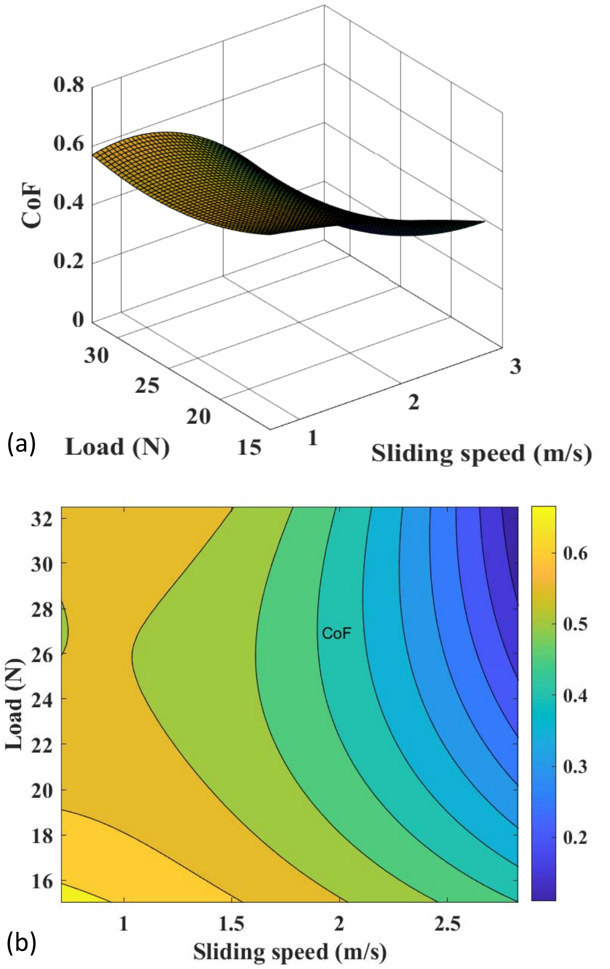

Figure 3. Interaction plots for CoF: (a) 3D surface plot and (b) 2D contour plot

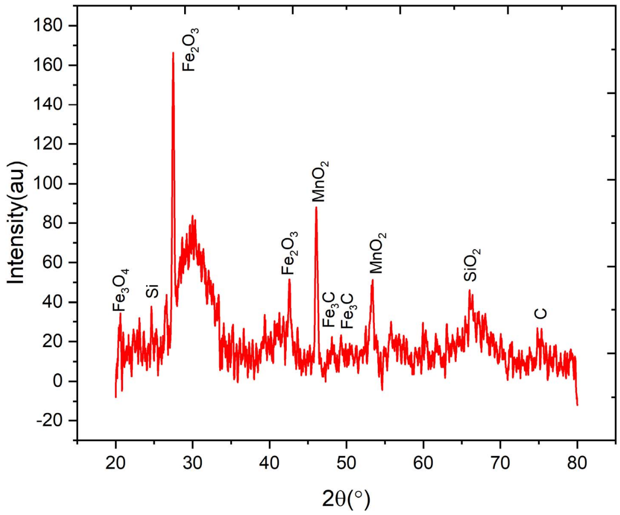

Figure 4. XRD peaks of the specimen with the highest wear rate worn-out surface

3.6 Worn surface microstructure analysis

Wear tracks are observed through the optical microscope. The ploughing direction is visible on the alloy with a dominant abrasive wear mechanism, as shown in Figure 5. The worn-out samples exhibit wear mechanisms such as ploughing, delamination and oxidation. The wear resistance is influenced by the extent of work hardening resulting from surface deformation.

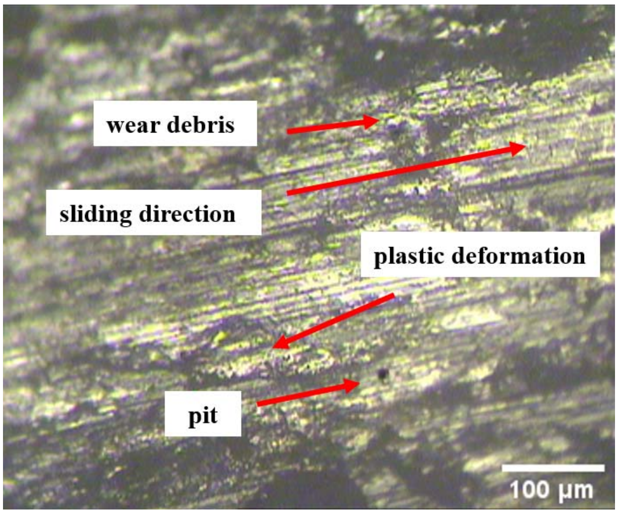

Figure 5. Optical microscope image of the specimen with the highest wear rate worn-out surface

The wear resistance of alloy depends on inherent material properties and the microstructure of microconstituents. The black patches represent the presence of ferritic structure in the composition of specimens. Hard microconstituents like carbides formed from reinforcing elements minimise the alloy steel's mass loss. The alloy steel's mass loss is reduced due to carbide formation, but it simultaneously increases the CoF due to contact with interacting metallic surfaces.

The microstructure of the severely worn-out test pin was also studied using SEM (JEOL JSM-6701F), as shown in Figure 6. The figure reveals that the test pin has undergone mainly non-uniform abrasive and adhesive wear, as well as material pull-outs at particular places where pores were present. The surface is rough and uneven, with many scratches, grooves and pits. This suggests that the material has been subjected to wear, likely by the hard-phase material. Adhesion and welding of the asperities of the mating surfaces result in adhesive wear and heat generation. This leads to an increase in surface roughness, causing higher friction. Abrasive wear could be observed on the worn-out surface of the specimen with the highest wear due to hard particles resulting from adhesive wear. The pits may have been caused by impacts from hard phases such as Fe_3C or by the removal of SiO_2 and MnO_2 from the surface. Carbon and other elemental powder additions improved the alloy steel specimens' strength and reduced the mass loss.

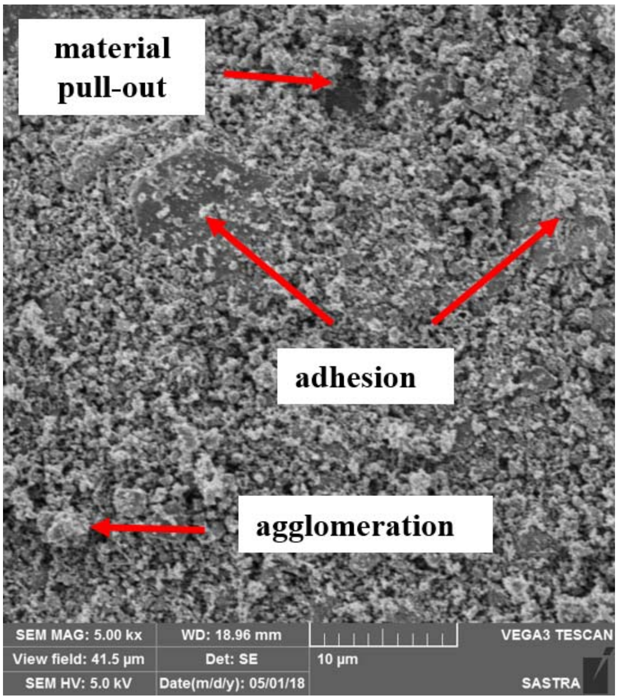

Figure 6. SEM image of the specimen with the highest wear rate microstructure

4. Conclusion

Alloy steel, whose chemical composition is close to EN24 alloy, was developed through the PM route from the Atomet 4601 + 0.35 C + 0.25 Mn + 0.1 Si + 0.9 Cr wt. % powders. Experimental test results are obtained after the standard experimental procedures. The tribological performance characteristics of alloy steel obtained through PM were studied with the aid of a computer-based data acquisition system of dry sliding friction and wear test rig. The influence of normal load and sliding speed on the response variables is studied through interaction plots.

For the various cases considered and quantified in experimental results, the wear rate varied from 0.32×10^{-3} to 1.02×10^{-3} mm^3/m. The lowest was at 15 N and 1.77 m/s and the highest was at 32.5 N and 2.83 m/s.

The coefficient of friction was the highest (0.673) at 15 N and 0.71 m/s. On the other hand, at the highest load (32.5 N) and sliding speed (2.83 m/s), the coefficient of friction was the lowest (0.1311).

Regression models for wear rate and coefficient of friction were obtained with an R^2 = 0.98 based on experimental results, which reveals the strong correlation between the response and the independent parameters.

Carbides and oxides embedded in the ferrite grain matrix were observed during XRD analysis.

The rough and uneven worn surface with many scratches, grooves and pits indicates that the material has been exposed to wear. Adhesive, abrasive and oxidative wear were the dominant wear mechanisms noticed.

Studying and quantifying the alloy steel's characteristics will help the PM designer in selecting suitable materials for new applications. There is a wider scope to enhance the performance of alloy steel, such as investigating the feasibility of PM alloy steel's use in high-temperature environments.

References

[1] P. Ramakrishnan, Powder Metallurgy of Automotive and High Performance Materials in Engineering Industries, New Age International, New Delhi, 2010.

[2] K.S. Narasimhan, Recent advances in ferrous powder metallurgy, Advanced Performance Materials, Vol. 3, No. 1, 1996, pp. 7-27, DOI: 10.1007/BF00136857

[3] C. Amsallem, A. Gaucher, G. Guilhot, The unlubricated frictional behaviour of sintered iron, Wear, Vol. 23, No. 1, 1973, pp. 97-112, DOI: 10.1016/0043-1648(73)90045-8

[4] T.K. Kandavel, R. Chandramouli, M. Manoj, B. Manoj, D.K. Gupta, Influence of copper and molybdenum on dry sliding wear behaviour of sintered plain carbon steel, Materials & Design, Vol. 50, 2013, pp. 728-736, DOI: 10.1016/j.matdes.2013.03.037

[5] T.K. Kandavel, R. Sravanesh, P. Karthikeyan, Optimization of working parameters on wear behaviour of the sinter-forged plain carbon steel, Proceedings of the Institution of Mechanical Engineers, Part B: Journal of Engineering Manufacture, Vol. 231, No. 8, 2017, pp. 1379-1388, DOI: 10.1177/0954405415592200

[6] X. Li, U. Olofsson, A study on friction and wear reduction due to porosity in powder metallurgic gear materials, Tribology International, Vol. 110, 2017, pp. 86-95, DOI: 10.1016/j.triboint.2017.02.008

[7] X. Li, J. Liu, J. Xiong, L. Yang, Q. Gou, X. Song, Z. Guo, T. Hua, M. Liang, Wear and corrosion resistant Mn-doped austenitic cast iron prepared by powder metallurgy method, Journal of Materials Research and Technology, Vol. 9, No. 3, 2020, pp. 6376-6385, DOI: 10.1016/j.jmrt.2020.03.099

[8] B. Singh, J.S. Grewal, Study of dry wear behavior of novel ferrous samples prepared by powder metallurgy method, Surface Topography: Metrology and Properties, Vol. 10, No. 2, 2022, Paper 025003, DOI: 10.1088/2051-672X/ac63d8

[9] M. Mamatha Kumari, S. Natarajan, J. Alphonsa, S. Mukherjee, Dry sliding wear behaviour of plasma nitrocarburised AISI 304 stainless steel using response surface methodology, Surface Engineering, Vol. 26, No. 3, 2010, pp. 191-198, DOI: 10.1179/174329409X439041

[10] S. Negi, S. Dhiman, R.K. Sharma, Investigating the surface roughness of SLS fabricated glass-filled polyamide parts using response surface methodology, Arabian Journal for Science and Engineering, Vol. 39, No. 12, 2014, pp. 9161-9179, DOI: 10.1007/s13369-014-1434-7

[11] N. Radhika, R. Raghu, Dry sliding wear behaviour of aluminium Al-Si12Cu/TiB_2 metal matrix composite using response surface methodology, Tribology Letters, Vol. 59, 2015, Paper 2, DOI: 10.1007/s11249-015-0516-3

[12] I. Saravanan, A. Elaya Perumal, S.C. Vettivel, N. Selvakumar, A. Baradeswaran, Optimizing wear behavior of TiN coated SS 316L against Ti alloy using response surface methodology, Materials & Design, Vol. 67, 2015, pp. 469-482, DOI: 10.1016/j.matdes.2014.10.051

[13] M. Emayavaramban, T.K. Kandavel, Effects of titanium (Ti) addition on wear behaviour of powder metallurgy (P/M) plain carbon steel, International Journal of Innovation and Scientific Research, Vol. 22, No. 2, 2016, pp. 384-394.

[14] T.K. Kandavel, T. Panneerselvam, V. Mohan, Experimental investigation on wear characteristics of sintered Fe-C-Cr low alloy steels, International Journal of Surface Science and Engineering, Vol. 11, No. 5, 2017, pp. 381-402, DOI: 10.1504/IJSURFSE.2017.088121

[15] N. Jeyaprakash, M. Duraiselvam, S.V. Aditya, Numerical modeling of WC-12% Co laser alloyed cast iron in high temperature sliding wear condition using response surface methodology, Surface Review and Letters, Vol. 25, No. 7, 2018, Paper 1950009, DOI: 10.1142/S0218625X19500094

[16] M. Venkat Krishna, T.K. Kandavel, K.P. Reddy, A. Jayaprakash, Experimental study on deformation and densification properties of sintered ATOMET 4601 + TiC alloy steels under cold upsetting, Pakistan Journal of Biotechnology, Vol. 14, No. 2, 2017, pp. 183-187.

[17] M. Venkat Krishna, T.K. Kandavel, K.P. Reddy, A. Jayaprakash, Weldability study on ATOMET 4601 + TiC alloy steels, International Journal of Pure and Applied Mathematics, Vol. 117, No. 16, 2017, pp. 465-473.

[18] K.P. Reddy, T.K. Kandavel, S. Nelson Raja, Workability and corrosion behavior studies on sintered iron-based hybrid powder metallurgy alloys, Materials and Corrosion, Vol. 73, No. 11, 2022, pp. 1854-1864, DOI: 10.1002/maco.202213268

[19] R.K. Khatirkar, P. Yadav, S.G. Sapate, Structural and wear characterization of heat treated EN24 steel, ISIJ International, Vol. 52, No. 7, 2012, pp. 1370-1376, DOI: 10.2355/isijinternational.52.1370

[20] M.S. Charoo, M.F. Wani, M. Hanief, A. Chetani, M.A. Rather, Tribological characteristics of EN8 and EN24 steel against aluminium alloy 6061 under lubricated condition, Advanced Materials Proceedings, Vol. 2, No. 7, 2017, pp. 445-449, DOI: 10.5185/amp.2017/709

[21] N.H. Dhanvij, S.H. Gawande, P.S. Gajjal, Performance evaluation of EN24 for planetary gear transmission of CNC bending machine, Journal of the Brazilian Society of Mechanical Sciences and Engineering, Vol. 42, 2020, Paper 298, DOI: 10.1007/s40430-020-02392-5

[22] N. Kumar, B. Ganguli, B. Roy, B. Deb, Investigation of surface properties of EN8, EN24, and EN41B low alloy steel treated by active screen plasma nitriding, Transactions of the Indian Institute of Metals, Vol. 74, No. 4, 2021, pp. 799-810, DOI: 10.1007/s12666-021-02191-z

[23] S.S. Dumne, B. Rajiv, M.D. Jaybhaye, Experimental investigation of EN24 steel against OHNS under wet sliding conditions by using pin-on-disc, in Proceedings of the 2nd Indian International Conference on Industrial Engineering and Operations Management, 16-18.08.2022, Warangal, India, pp. 1148-1158, DOI: 10.46254/IN02.20220345

[24] E.R. Leheup, D. Zhang, J.R. Moon, Low amplitude reciprocating wear of sintered iron, Wear, Vol. 176, No. 1, 1994, pp. 121-130, DOI: 10.1016/0043-1648(94)90205-4

[25] B. Bhushan, Introduction to Tribology, John Wiley & Sons, New York, 2013, DOI: 10.1002/9781118403259

[26] N.P. Suh, An overview of the delamination theory of wear, Wear, Vol. 44, No. 1, 1977, pp. 1-16, DOI: 10.1016/0043-1648(77)90081-3

[27] S. Kang, A study of friction and wear characteristics of copper- and iron-based sintered materials, Wear, Vol. 162-164, No. B, 1993, pp. 1123-1128, DOI: 10.1016/0043-1648(93)90131-5